Icarus 226 (2013) 1612–1617

Contents lists available at ScienceDirect

Icarus

journal homepage: www.elsevier.com/locate/icarus

Note

Reflectance spectroscopy (200–2500 nm) of highly-reduced phases under oxygen- and water-free conditions

M.R.M. Izawa [a,*], D.M. Applin [a], P. Mann [a], M.A. Craig [b], E.A. Cloutis [a], J. Helbert [c], A. Maturilli [c]

[a] Hyperspectral Optical Sensing for Extraterrestrial Reconnaissance Laboratory, Dept. Geography, University of Winnipeg, 515 Portage Avenue, Winnipeg, Manitoba R3B 2E9, Canada
[b] Dept. Earth Sciences, Centre for Planetary Science and Exploration, Western University, 1151 Richmond St., London, Ontario N6A 5B7, Canada
[c] Deutsche Zentrum für Luft- und Raumfahrt (German Aerospace Center), Institute of Planetary Research, Experimental Planetary Physics, Rutherfordstraße 2, 12489 Berlin, Germany

ARTICLE INFO

Article history:
Received 6 May 2013
Revised 20 June 2013
Accepted 12 August 2013
Available online 19 August 2013

Keywords:
Asteroids, surfaces
Spectroscopy
Asteroids, composition
Ultraviolet observations
Mercury, surface

ABSTRACT

Spectra of highly-reduced mineral phases from 200 to 2500 nm provide new laboratory constraints on the surfaces of asteroids and other extremely reduced solid assemblages. Synthetic oldhamite (CaS) is distinguished by high ultraviolet reflectance (which decreases toward shorter wavelengths). Oldhamite and osbornite spectra show absorption features at ~401 nm and ~436 nm, respectively. Chemically pure synthetic oldhamite is spectrally distinct from naturally-occurring oldhamite from the Norton County aubrite, possibly due to differences in minor and trace element compositions, presence or absence of inclusions, or differences in oxidation/hydration (terrestrial weathering). Iron powders at 50 nm and 10 μm nominal particle sizes, nanophase graphite, and carlsbergite (CrN) all have very low reflectivity over the 200–2500 nm wavelength range. Carlsbergite has a slight blue spectral slope in the visible and near-infrared (400–2500 nm), while the iron powders and nanophase graphite show slight red slopes over this wavelength range.

1. Introduction

Some common extraterrestrial minerals are extremely rare or absent in Earth materials. Important planetary materials, including oldhamite and nanophase iron, oxidize and hydrolyze rapidly in contact with Earth's atmosphere and hydrosphere (e.g., Cooper et al., 2012; Haberle et al., 2013; Okada et al., 1981). Oldhamite is particularly susceptible to terrestrial weathering, and is rapidly altered to sulfates (bassanite, gypsum), oxhydroxides (portlandite), and carbonates (vaterite, calcite) as described by Okada et al. (1981). Nitrides and graphite are less reactive, but may still be affected by adsorbed atmospheric water or gases. We have conducted a spectroscopic study of synthetic versions of CaS (oldhamite), TiN (osbornite), CrN (carlsbergite), nanophase graphite, and iron (10 μm and 50 nm nominal particle sizes) under an oxygen-free anhydrous N_2 atmosphere. In the subsequent discussion we use the mineralogic terms for these synthetic equivalents unless otherwise indicated. Given the considerable uncertainty concerning the extent to which known meteorites are representative of the asteroids, and the lack of any known meteorites that sample of the surface of Mercury, spectral studies of diverse highly-reduced materials are useful for understanding the properties of planetary surfaces using telescopic, orbiter and lander data sets. Objects which may contain highly-reduced mineral assemblages include the parent asteroids of enstatite chondrites, aubrites, iron meteorites, pallasites, mesosiderites (or similar materials not present in terrestrial meteorite collections), and the surface of Mercury.

2. Methods

The samples used in this study are described in Table 1. All of the samples are air-sensitive. Special procedures were implemented to preserve their integrity. Spectra were collected in a Plas-Labs 818 GBB glovebox with interior dimensions of $152.4W \times 96.5D \times 79H$ cm (Plas-labs Inc., Lansing, MI) under a dry N_2 atmosphere, where dry nitrogen was passed through a series of Drierite filters. The glovebox also contained Drierite and Chemisorb to remove any remaining water and CO_2. Humidity and CO_2 levels were monitored continuously, and remained $\ll$1% throughout the measurements. Samples were only opened within the glovebox and were exposed to the glove box atmosphere for minutes at most. Possible oxidation and hydration were monitored by periodically measuring spectra of samples of 50 nm nanophase iron and oldhamite that were left exposed within the glovebox. If oxygen or water vapor were present, they would produce Fe-oxyhydroxides from the nanophase iron and Ca-sulfates from the oldhamite, which would be detectable via Fe–O charge-transfer transitions, or overtones of O–H or S–O vibrational features. Because no such spectral features were detected, we are confident that contamination from, or alteration by, Earth's atmosphere did not occur and did not affect our data set.

* Corresponding author.
E-mail address: matthew.izawa@gmail.com (M.R.M. Izawa).

0019-1035/$ - see front matter © 2013 Elsevier Inc. All rights reserved.
http://dx.doi.org/10.1016/j.icarus.2013.08.014

Table 1
Sample descriptions.

Mineral name	Ideal chemical formula	HOSERLab sample ID	Notes
Oldhamite	CaS	CAS001	Calcium sulfide, synthetic CaS; 99.9% (metals basis excluding Sr) Sr typically 500 ppm; CAS #20548-54-3. Alfa Aesar stock number 13121, lot #G16U051, −325 mesh powder. 5 g packed under argon
Osbornite	TiN	TIN001	Titanium nitride (TiN), synthetic. 99.5% (metals basis), Alfa Aesar stock number 41556-18, lot #X29S045. CAS #25583-20-4
Carlsbergite	CrN	CAR101	Carlsbergite: synthetic CrN (ESPI Corp., #K1367R)
Graphite, nanophase	C	GRP200	Graphite nanopowder; synthetic (MTI Corporation); <30 nm particle size; 99.5% purity, non-crystalline; >60 m^2/g specific surface area
Iron, Britt-Pieters particles	Fe	IRO103	Iron, synthetic powder, spherical, <10 μm, 99.9%+ (metals basis), 99.5% (Alfa Aesar stock #00170-14, 62-03-02; lot #L05R011)
Iron, nanophase	Fe	IRO102	Iron, synthetic nanophase; average particle size <50 nm. MTI Corporation. PCVD manufacturing method. Packed under vacuum. 40–60 m^2/g surface area

We have consistently used the mineral names of the synthetic compounds (e.g., oldhamite for CaS, osbornite for TiN) because these synthetic compounds are crystallographically and chemically equivalent to idealized (without impurities) versions of the corresponding natural minerals. Chemical substitutions in the natural minerals (e.g., minor substitution of Mg^{2+} or Sr^{2+} for Ca^{2+} in oldhamite) will not significantly change the crystal structures.

2.1. 350–2500 nm measurements (near UV, VIS, and near IR regions)

The 350–2500 nm reflectance spectra were measured with an Analytical Spectral Devices FieldSpec Pro HR spectrometer which acquires data from 350 to 2500 nm in 1.4 nm steps, with a spectral resolution of between 2 and 7 nm. The data are internally resampled by the instrument to output data ultimately at 1 nm intervals. Data below approximately 400 nm may be affected by low signal levels and hence data in the 350–400 nm region, particularly the abrupt changes in slope, are suspect. Unless otherwise indicated, spectra were measured at a viewing geometry of $i = 30°$ and $e = 0°$. Incident light was provided by an in-house 100 W quartz–tungsten–halogen collimated light source. Sample spectra were measured relative to a Spectralon (Labsphere, North Sutton, NH) standard and corrected for minor (less than ~2%) irregularities in its absolute reflectance. In each case, 200 spectra of the dark current, standard, and sample were acquired and averaged, to provide sufficient signal-to-noise for subsequent interpretation. Locations of reflectance minima in oldhamite and osbornite were determined by fitting a 3rd-order polynomial to the measured spectra.

2.2. 200–400 nm measurements (UV region)

The ultraviolet spectroscopy methods used in this study were initially described by Cloutis et al. (2008) and are briefly summarized here. The 200–400 nm spectra were measured with an Ocean Optics S-2000 spectrometer equipped with a grating that provides coverage from 200 to 859 nm with spectral resolution between 0.36 nm (at 200 nm) and 0.28 nm (at 859 nm). Illumination was provided by an Analytical Instrument Systems Inc. Mini-DTA light source with output from a 30 W deuterium lamp directed through a bifurcated fiber optic bundle consisting of six illumination fibers surrounding a central pick-up fiber feeding into the detector array. This assembly consisted of 400-μm diameter solarization-resistant (XSR) fibers, with transmission efficiencies between 23% and 40% across the 200–400 nm range. The fiber optic bundle was used in normal incidence and we used an integration time of 1000 ms and averaged 100 individual spectra. Measurements for each sample were made by first acquiring a dark current spectrum (with the input to the spectrometer blocked), a reference spectrum of our $BaSO_4$ standard (Alfa Aesar Puratronic grade: 99.998% metals basis; CAS #7727-43-7), followed by measurement of the samples. All three measurements were made using an identical viewing geometry, integration time, and number of averaged spectra. The reference and target were both placed at the same distance from the end of the fibers bundle (~5 mm). The fibers have a 25.4° field of view, and this working distance provided the best compromise between measurement time, uniform target illumination, and size of the sample being imaged. The most appropriate definition of the instrument configuration is a biconical arrangement with i and e centered on ~0° and detector and illumination fields of view of 25.4°. The spectra were corrected for irregularities in the $BaSO_4$ standard using a calibrated deep UV mirror as described in Cloutis et al. (2008).

2.3. Note on terminology for fine iron particles

Various terms have been used in the planetary science literature for very small iron particles thought to influence the spectral properties of airless bodies, including nanophase iron ($npFe^0$) (Keller and McKay, 1993; Pieters et al., 2000), submicroscopic metallic iron (SMFe) (Hapke, 2001), and Britt-Pieters particles or microphase iron (Lucey and Riner, 2011; Riner and Lucey, 2012). In the present study, we have used commercially available iron powders of 50 nm and 10 μm particle sizes. The 50 nm powder consists of nanophase iron, applying the widely accepted definition adopted by the American Society for Testing and Materials (ASTM) "nanoparticle: sub-classification of ultrafine particle with lengths in two or three dimensions greater than 0.001 μm (1 nm) and smaller than about 0.1 μm (100 nm) and which may or may not exhibit a size-related intensive property" (ASTM, 2012). The 10 μm powder would be classified as a coarse particle according the ASTM definition "a particle smaller than about 10 μm and larger than about 2.5 μm in size" (ASTM, 2012). For the 50 nm powder, we have used

Table 2
Albedo and reflectance ratio measurements.

Sample ID	Albedo (560 nm) (%)	Reflectance ratios (wavelength positions given in nm)				
		2400/560	600/500	1800/800	1800/1250	1250/600
CAS001 (oldhamite)	62.35	1.12	1.07	1.02	1.00	1.08
TIN001 (osbornite)	10.59	2.95	2.17	1.36	1.06	2.18
CAR101 (carlsbergite)	5.33	0.67	1.01	0.80	0.81	1.03
GRP200 (np graphite)	0.97	1.23	0.94	0.89	0.98	0.83
IRO103 (np iron, 10 μm)	2.81	1.48	0.98	1.00	1.00	0.99
IRO102 (np iron, 50 nm)	2.60	1.23	0.97	0.91	0.98	0.92

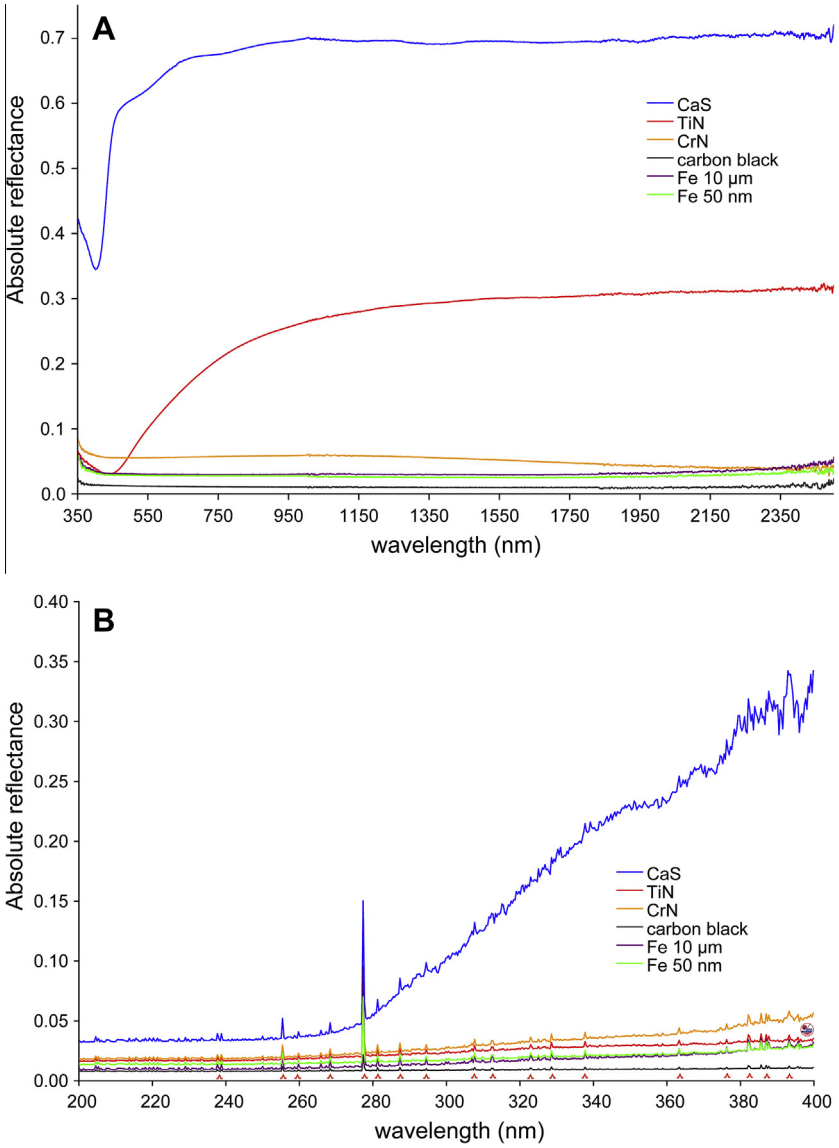

Fig. 1. Absolute reflectance spectra of CaS (oldhamite, CAS001), TiN (osbornite, TIN001), CrN (carlsbergite, CAR101), nanophase graphite (carbon black, GRP200) and iron powders: 10 μm Britt-Pieters particles (IRO103), and 50 nm nanophase iron (IRO102). (A) Near-UV, visible and near infrared spectra collected with $i = 30°$ and $e = 0°$, absolute reflectance. (B) Ultraviolet spectra collected with $i = 0°$ and $e = 0°$, with the reflectance of each spectrum at 400 nm scaled to match the reflectance measured by the ASD spectrometer at 400 nm. The narrow peaks in the UV spectra (positions denoted with small symbols below) are attributable the deuterium light source (Cloutis et al., 2008).

the term nanophase iron. For the 10 μm powder, we have used the term Britt-Pieters particles following (Lucey and Riner, 2011; Riner and Lucey, 2012). Where both iron particle sizes are referred to simultaneously, we have used the term iron powder.

3. Results

3.1. 350–2500 nm observations (near UV, VIS, and near IR)

Spectral slope is here defined as the ratio of reflectance at 2500 nm to that at 560 nm. Albedo and spectral slope parameters are summarized in Table 2, following (Cloutis et al., 2010). Oldhamite has a high albedo (62.35% at 560 nm) and a strong absorption feature with a minimum near 401 nm and shoulders centered near 546 nm and 763 nm, and possible weak features at ~1150 nm and ~1380 nm. Osbornite has an absorption feature with a minimum near ~436 nm and 10.59% reflectance at 560 nm (Fig. 1A and B). Carlsbergite is dark (5.33% reflectance at 560 nm) and is spectrally featureless with a blue slope (Fig. 1A and B). Neither of these phases has been spectrally characterized before.

Iron powders, at both 10 μm and 50 nm nominal particle sizes, have dark (2.81% and 2.60% reflectance at 560 nm respectively) and featureless spectra with nearly flat to slightly red spectral slopes (Fig. 1A and B; cf. Fig. 5d of Noble et al. (2007), for ~50 nm particles). The similar spectral properties of these two iron particle sizes are somewhat surprising as the finer-grained sample is expected to be more red-sloped than the larger size (Lucey and Riner, 2011). It is likely that the similar spectral slopes are due to the fact that we are measuring pure powders as opposed to grains dispersed in a more transparent matrix (Noble et al., 2007). It is possible that the 50 nm particles are aggregating to create much larger effective particle sizes, as Rayleigh scattering would be expected to dominate for 50 nm particles, as the size parameter $\pi D/\lambda$ is less than unity for the entire wavelength range studied here (Lucey and Riner, 2011). Nanophase graphite has extremely low albedo (0.97% at 560 nm), is spectrally featureless, and has a slight red slope (Fig. 1A and B). Its spectral properties are similar to other graphites that have been spectrally characterized, all of which show red-sloped spectra with a minimum in the 0.7 μm region (Cloutis et al., 1990, 1994). The lack of a minimum near 0.7 μm and the overall

shape of graphite spectra are very sensitive to small differences in composition and structure (e.g., Blanco et al., 1988; Bussoletti et al., 1978; Draine, 1985; Rouleau and Martin, 1991).

3.2. 200–400 nm observations (UV)

Osbornite, carlsbergite, nanophase graphite and both iron powders have monotonically increasing reflectance with increasing wavelength in the ultraviolet (Fig. 1C). Oldhamite is distinguished by a high reflectance in the ultraviolet and by weak inflections or shoulders near ~360 nm and 375 nm (Fig. 1C).

4. Discussion

All the materials studied here have monotonically increasing reflectance with increasing wavelength in the ultraviolet. Osbornite, carlsbergite, nanophase graphite and the iron powders all have low reflectance from 200 to 400 nm. Oldhamite is distinctive and has a high reflectance in the near ultraviolet, increasing from ~4.5% at 275 nm to ~34% at 400 nm. The high ultraviolet reflectance of oldhamite could facilitate remote detection. Spectra of pure oldhamite in the 350–2500 nm range in the present study are markedly different from those of Burbine et al. (2002). Similar to the results by Helbert et al. (2013), our spectra do not show the absorptions at ~490 and ~950 nm, and instead show a single strong absorption centered near 401 nm with shoulders centered near 546 nm and 763 nm and possible weak features at ~1150 nm and ~1380 nm (cf. Fig. 1 of this study with Fig. 3 of Burbine et al., 2002). The oldhamite investigated in this study is synthetic and close to chemically pure (99.9%, 500 ppm Sr; see Table 1), while that measured by Burbine et al. (2002) was naturally-occurring oldhamite from the Norton County aubrite, which contains trace amounts of other transition elements, including 0.94 wt.% Mn (Okada et al., 1988). Okada et al. (1988) and Wheelock et al. (1994) found that the Fe content of Norton County oldhamite was below the detection limit of the electron probe microanalyzer (~0.02 wt.%), but these studies report only one and four analyses respectively. Oldhamite from other enstatite meteorites includes up to several wt.% Fe (e.g., Brearley and Jones, 1998; Mittlefehldt et al., 1998), therefore it is probable that some Norton County oldhamite also contains Fe. The ~490 nm and ~950 nm spectral features in the Norton County oldhamite may therefore be due to crystal field transitions of Fe^{2+} (and to a lesser extent Mn^{2+}) octahedrally co-ordinated to S^{2-} in oldhamite (Okada et al., 1980, 1988). Oldhamite separated from the Norton County aubrite may also have contained inclusions of other sulfides including troilite, daubreelite, alabandite, schollhornite and caswellsilverite (Okada and Keil, 1982; Okada et al., 1980, 1985, 1988); such inclusions may also contribute to the spectral features at ~490 and ~950 nm. Norton County has been subjected to terrestrial weathering, and oldhamite is particularly susceptible to alteration, therefore some spectral features of Norton County oldhamite may be related to weathering products including portlandite, vaterite, calcite, bassanite, and gypsum (Okada et al., 1981).

The oldhamite absorption feature near 401 nm is likely due to charge transfer between the valance band (S 3p orbitals) and the conduction band (empty Ca 3p, Ca 4s and S 3p σ^* antibonding orbitals) (Fleet, 2005). Shoulders at 546 nm and 763 nm and weak possible features at 1151 nm and 1381 nm may be attributable to the crystal field transitions of Ca^{2+} octahedrally co-ordinated to S^{2-} (Burns, 1993; Fleet, 2005).

To the best of our knowledge, reflectance spectra of osbornite and carlsbergite have not previously been measured over the wavelength range studied here. Osbornite (TiN) shows a visible absorption feature centered near 436 nm, probably due to charge transfer between the valance and conduction bands (N $2p_\pi \rightarrow$ Ti $3d_{xy}$) (Kuznetsov and Serpone, 2009; Patsalas and Logothetidis, 2001).

Observable spectral changes other than the appearance of absorption features can be caused by the presence of opaque materials like those studied here. For instance, finely-dispersed opaque phases can greatly darken a material and reduce the contrast of spectra features and can induce large changes in spectral slope (e.g., Clark, 1983; Cloutis et al., 2011; Milliken and Mustard, 2007).

4.1. Potential for detection on planetary surfaces

Oldhamite is the most likely candidate for remote detection based on its spectral characteristics including high UV reflectance and detectable spectral features in the visible and near-IR. Oldhamite-rich lithologies (commonly occurring as clasts or veins) are known from several enstatite meteorites including the Abee EH4 impact melt breccia (Rubin and Keil, 1983), the EL6 chondrite Jajh deh Kot Lalu (Rubin et al., 1997), the Norton County aubrite (Wheelock et al., 1994), and the Bustee aubrite (McCoy, 1998). Oldhamite is likely the product of impact melts on enstatite meteorite parent bodies (e.g., Rubin and Keil, 1983; Rubin et al., 1997). Oldhamite may be more abundant on some E-type asteroids, for instance, an oldhamite abundance of up to 42% has been suggested by Nedelcu et al. (2007) for Asteroid 2867 Steins. Clark et al. (2004) concluded from spectroscopic observations and compositional modeling that several E-type asteroids contain abundant sulfides, possibly including oldhamite, and that several E-types may not correspond with known enstatite-rich meteorites (E chondrites or aubrites). Oldhamite-rich lithologies may be widespread on the surface of Mercury. Direct measurements of the S concentration of the Hermean crust by the MErcury Surface, Space ENvironment, GEochemistry, and Ranging (MESSENGER) gamma ray and X-ray spectrometers showed high S abundances (estimated concentrations of ~4 wt.%) and correlations of Mg and Ca with S suggestive of sulfide-rich lithologies (Evans et al., 2012; Nittler et al., 2011; Weider et al., 2011; Zolotov et al., 2013). The MESSENGER findings confirmed previous suggestions based primarily on radar observations for S-rich materials on Mercury's surface (e.g., Sprague et al., 1995). Separation of CaS from sulfide melts by liquid immiscibility has been documented in both synthetic and natural systems (e.g., Floss et al., 1998; Skinner and Luce, 1971; Wheelock et al., 1994). Sulfide liquid immiscibility could therefore produce local enrichments of oldhamite in a variety of settings including impact melts (as melt sheets, ponds, and veins) and endogenic igneous rocks (e.g., Floss et al., 1998; Helbert et al., 2013; Wheelock et al., 1994). The thermal breakdown of sulfide minerals at subsolidus temperatures may play a role in the formation of 'hollows' on the surface of Mercury (Blewett et al., 2012; Helbert et al., 2013).

Osbornite is a trace constituent of many enstatite chondrites (e.g., Rubin, 1997), and has been reported in an oldhamite-rich lithology from the Bustee aubrite (McCoy, 1998). Osbornite, likely formed as an early Solar System condensate, has also been reported from comet Wild-2 (Chi et al., 2009). Carlsbergite is a fine-grained trace constituent of many iron meteorites (e.g., Axon et al., 1981; Buchwald and Scott, 1971).

4.2. Stellar envelopes and disks

Another, more speculative setting in which to search for spectral signatures for highly-reduced minerals is in extrasolar, astrophysical settings such as stellar disks and supernova outflows. Presolar diamonds, carbides and nitrides have been observed in primitive meteorites (e.g., Meibom et al., 2007; Nittler et al., 1995) and from comets (Chi et al., 2009). Recently, presolar oldhamite was identified as an inclusion in an SiC grain originating from

an Asymtotic Giant Branch (AGB) star (Hynes et al., 2011). The probable low concentrations of sulfides and nitrides would make detection difficult, however, both crystalline and amorphous silicates have been identified in stellar outflows (e.g., Gail et al., 2009), thus it is not inconceivable that other solid phases including some of those investigated here could also be detected under favorable circumstances. Therefore, while the spectra reported here are not directly comparable to those of dust in stellar envelopes, they may still provide some constraints on the presence of highly-reduced phases in astrophysical settings.

5. Conclusions

The highly-reduced phases studied here are characterized by a range of reflectance values, with oldhamite and osbornite having higher reflectance than the other highly-reduced phases. The presence of absorption features in these two materials opens up the possibility of their being spectrally detectable using these features. The differences in spectral properties between synthetic and meteoritic oldhamite suggests that it is possible to determine compositional variations in this material from spectral variations. It is also possible that differences in spectral properties between different subgroups of E-class asteroids (Clark et al., 2004) may be attributable to variations in oldhamite and other sulfides on these bodies.

Acknowledgments

MRMI acknowledges funding from the NSERC CREATE Canadian Astrobiology Training Program and the Mineralogical Association of Canada. The University of Winnipeg's HOSERLab was established with funding from the Canada Foundation for Innovation, the Manitoba Research Innovations Fund and the Canadian Space Agency, whose support is gratefully acknowledged. This study was supported by research grants from NSERC, the Canadian Space Agency and the University of Winnipeg. Thanks to Miriam Riner and an anonymous reviewer for their constructive comments which greatly improved this manuscript, and to Will Grundy for editorial handling. This research has made use of NASA's Astrophysics Data System.

References

ASTM E2456-06, 2012. Standard Terminology Relating to Nanotechnology. American Society for Testing and Materials.
Axon, H.J. et al., 1981. Carlsbergite, CrN, in troilite, FeS, of the Sikhote Alin meteoritc iron. Miner. Mag. 44, 107–109.
Blanco, A. et al., 1988. A mixture of hydrogenated amorphous carbon grains and PAH molecules: A candidate for the unidentified infrared bands? Astrophys. J. 334, 875–882.
Blewett, D.T. et al., 2012. Mercury's hollows: Constraints on formation and composition from analysis of geological setting and spectral reflectance. J. Geophys. Res. 118, 1–20.
Brearley, A.J., Jones, R.H., 1998. Chondritic meteorites. In: Papike, J.J. (Ed.), Planetary Materials. Mineralogical Society of America, Washington, DC, p. 398.
Buchwald, V.F., Scott, E.R.D., 1971. First nitride (CrN) in iron meteorites. Nat. Phys. Sci. 233, 113–114.
Burbine, T.H. et al., 2002. Spectra of extremely reduced assemblages: Implications for Mercury. Meteorit. Planet. Sci. 37, 1233–1244.
Burns, R.G., 1993. Mineralogical Applications of Crystal Field Theory. Cambridge University Press, London.
Bussoletti, E. et al., 1978. Tabulated extinction efficiencies for various types of submicron amorphous carbon grains in the wavelength range 1000 Å–300 μm. Astron. Astrophys. 70, 257–268.
Chi, M. et al., 2009. The origin of refractory minerals in Comet 81P/Wild 2. Geochim. Cosmochim. Acta 73, 7150–7161.
Clark, R.N., 1983. Spectral properties of montmorillonite and dark carbon grains: Implications for remote sensing minerals containing chemically and physically adsorbed water. J. Geophys. Res. 88, 10635–10644.
Clark, B.E. et al., 2004. E-type asteroid spectroscopy and compositional modeling. J. Geophys. Res. 109, 1–11.
Cloutis, E.A. et al., 1990. Reflectance spectra of 'featureless' materials and the surface mineralogies of M- and E-class asteroids. J. Geophys. Res. 95, 281–293.
Cloutis, E.A. et al., 1994. Spectral reflectance properties of carbon-bearing materials. Icarus 107, 276–287.
Cloutis, E.A. et al., 2008. Ultraviolet spectral reflectance properties of common planetary materials. Icarus 197, 321–347.
Cloutis, E.A. et al., 2010. Reflectance spectra of iron meteorites: Implications for spectral identification of their parent bodies. Meteorit. Planet. Sci. 45, 304–332.
Cloutis, E.A. et al., 2011. Spectral reflectance properties of carbonaceous chondrites: 2. CM chondrites. Icarus 216, 309–346.
Cooper, G. et al., 2012. Radar-enabled recovery of the Sutter's Mill meteorite, a carbonaceous chondrite regolith breccia. Science 338, 1583–1587.
Draine, B.T., 1985. Tabulated optical properties of graphite and silicate grains. Astron. J. Suppl. Ser. 57, 587–594.
Evans, L.G. et al., 2012. Major-element abundances on the surface of Mercury: Results from the MESSENGER Gamma-ray Spectrometer. J. Geophys. Res. 117, E00L07.
Fleet, M.E., 2005. XANES spectroscopy of sulfur in Earth materials. Can. Miner. 43, 1811–1838.
Floss, C. et al., 1998. Sulfide/silicate melt partitioning during enstatite chondrite melting. Meteorit. Planet. Sci. 33, A51–A52.
Gail, H.-P. et al., 2009. Stardust from asymptotic giant branch stars. Astrophys. J. 698, 1136–1154.
Haberle, C.W. et al., 2013. Calcium–sulfur–chlorine-bearing phases within Sutter's Mill sample SM3 (pre-rain). Lunar Planet. Sci. 44.
Hapke, B., 2001. Space weathering from Mercury to the asteroid belt. J. Geophys. Res. 106, 10039–10073.
Helbert, J. et al., 2013. Visible and near-infrared reflectance spectra of thermally processed synthetic sulfides as a potential analog for the hollow-forming materials on Mercury. Earth Planet. Sci. Lett. 369, 233–238.
Hynes, K.M. et al., 2011. Combined TEM and nanoSIMS analysis of subgrains in an SiC Ab grain. Lunar Planet. Sci. 42.
Keller, L.P., McKay, D.S., 1993. Discovery of vapor deposits in the lunar regolith. Science 261, 1305–1307.
Kuznetsov, V.N., Serpone, N., 2009. On the origin of the spectral bands in the visible absorption spectra of visible-light-active TiO_2 specimens analysis and assignments. J. Phys. Chem. C 113, 15110–15123.
Lucey, P.G., Riner, M.A., 2011. The optical effects of small iron particles that darken but do not redden: Evidence of intense space weathering on Mercury. Icarus 212, 451–462.
McCoy, T.J., 1998. A pyroxene–oldhamite clast in Bustee: Igneous aubritic oldhamite and a mechanism for the Ti enrichment in aubritic troilite. Antarct. Meteorite Res. 11, 32–48.
Meibom, A. et al., 2007. Nitrogen and carbon isotopic composition of the Sun inferred from a high-temperature solar nebular condensate. Astrophys. J. 656, L33–L36.
Milliken, R.E., Mustard, J.F., 2007. Estimating the water content of hydrated minerals using reflectance spectroscopy. I. Effects of darkening agents and low-albedo materials. Icarus 189, 550–573.
Mittlefehldt, D.W. et al., 1998. Non-chondritic meteorites from asteroidal bodies. In: Papike, J.J. (Ed.), Planetary Materials.
Nedelcu, D.A. et al., 2007. E-type Asteroid (2867) Steins: Flyby target for Rosetta. Astron. Astrophys. 473, L33–L36.
Nittler, L.R. et al., 1995. Silicon nitride from supernovae. Astrophys. J. 453, L25–L28.
Nittler, L.R. et al., 2011. The major-element composition of Mercury's surface from MESSENGER X-ray spectrometry. Science 333, 1847–1850.
Noble, S.K. et al., 2007. An experimental approach to understanding the optical effects of space weathering. Icarus 192, 629–642.
Okada, A., Keil, K., 1982. Caswellsilverite, Nacrs2 – A new mineral in the Norton County enstatite achondrite. Am. Miner. 67, 132–136.
Okada, A. et al., 1980. The Norton-County enstatite achondrite – A brecciated, plutonic igneous rock. Meteoritics 15, 345–346.
Okada, A. et al., 1981. Unusual weathering products of oldhamite parentage in the Norton County enstatite achondrite. Meteoritics 16, 141–152.
Okada, A. et al., 1985. Schollhornite, $Na_{0.3}(H_2O)_1[CrS_2]$, a new mineral in the Norton County enstatite achondrite. Am. Miner. 70, 638–643.
Okada, A. et al., 1988. Igneous history of the aubrite parent asteroid – Evidence from the Norton-County enstatite achondrite. Meteoritics 23, 59–74.
Patsalas, P., Logothetidis, S., 2001. Optical, electronic, and transport properties of nanocrystalline titanium, nitride thin films. J. Appl. Phys. 90, 4725–4734.
Pieters, C.M. et al., 2000. Space weathering on airless bodies: Resolving a mystery with lunar samples. Meteorit. Planet. Sci. 35, 1101–1107.
Riner, M.A., Lucey, P.G., 2012. Spectral effects of space weathering on Mercury: The role of composition and environment. Geophys. Res. Lett. 39, L12201.
Rouleau, F., Martin, P.G., 1991. Shape and clustering effects on the optical properties of amorphous carbon. Astrophys. J. 377, 526–540.
Rubin, A.E., 1997. Mineralogy of meteorite groups. Meteorit. Planet. Sci. 32, 231–247.
Rubin, A.E., Keil, K., 1983. Mineralogy and petrology of the Abee enstatite chondrite breccia and its dark inclusions. Earth Planet. Sci. Lett. 62, 118–131.
Rubin, A.E. et al., 1997. Shock metamorphism of enstatite chondrites. Geochim. Cosmochim. Acta 61, 847–858.
Skinner, B.J., Luce, F.D., 1971. Solid solutions of the type (Ca,Mg,Mn,Fe)S and their use as geothermometers for the enstatite chondrites. Am. Miner. 56, 1269–1296.

Sprague, A. et al., 1995. Sulfur at Mercury: Elemental at the poles and sulfides in the regolith. Icarus 118, 211–215.
Weider, S.Z. et al., 2011. Chemical heterogeneity on Mercury's surface revealed by the MESSENGER X-ray Spectrometer. J. Geophys. Res. – Planets 117, E00L05.
Wheelock, M.M. et al., 1994. Ree geochemistry of oldhamite-dominated clasts from the Norton County aubrite – Igneous origin of oldhamite. Geochim. Cosmochim. Acta 58, 449–458.
Zolotov, M.Y. et al., 2013. The redox state, FeO content, and origin of sulfur-rich magmas on Mercury. J. Geophys. Res. 118, 138–146.